International Journal on Artificial Intelligence Tools
Vol. XX, No. X (2014) 1–27

World Scientific
www.worldscientific.com

EVALUATION OF IMAGE FORGERY DETECTION USING MULTI-SCALE WEBER LOCAL DESCRIPTORS

MUHAMMAD HUSSAIN

Department of Computer Science, College of Computer and Information Sciences,
King Saud University, Riyadh 11543, Saudi Arabia
mhussain@ksu.edu.sa

SAHAR QASEM

Department of Computer Science, College of Applied Sciences,
Taiz University, Taiz, Republic of Yemen
sahar.qasim2009@gmail.com

GEORGE BEBIS

Department of Computer Science and Engineering, University of Nevada, Reno, USA
bebis@cse.unr.edu

GHULAM MUHAMMAD

Department of Computer Engineering, College of Computer and Information Sciences,
King Saud University, P.O. Box 51178, Riyadh 11543, Saudi Arabia
ghulam@ksu.edu.sa

HATIM ABOALSAMH, HASSAN MATHKOUR

Department of Computer Science, College of Computer and Information Sciences,
King Saud University, P.O. Box 51178, Riyadh 11543, Saudi Arabia
{hatim, Mathkour} @ksu.edu.sa

Received (Day Month Year)
Revised (Day Month Year)
Accepted (Day Month Year)

Due to the maturing of digital image processing techniques, there are many tools that can forge an image easily without leaving visible traces and lead to the problem of the authentication of digital images. Based on the assumption that forgery alters the texture micro-patterns in a digital image and texture descriptors can be used for modeling this change; we employed two stat-of-the-art local texture descriptors: multi-scale Weber's law descriptor (multi-WLD) and multi-scale local binary pattern (multi-LBP) for splicing and copy-move forgery detection. As the tamper traces are not visible to open eyes, so the chrominance components of an image encode these traces and were used for modeling tamper traces with the texture descriptors. To reduce the dimension of the feature space and get rid of redundant features, we employed locally learning based (LLB) algorithm. For identifying an image as authentic or tampered, Support vector machine (SVM) was used. This paper presents the thorough investigation for the validation of this forgery detection method. The experiments were conducted on three benchmark image data sets, namely, CASIA v1.0, CASIA v2.0, and Columbia color. The experimental results showed that the accuracy rate of multi-WLD based method was 94.19% on CASIA v1.0, 96.52% on CASIA v2.0, and 94.17% on Columbia data

set. It is not only significantly better than multi-LBP based method, but also it outperforms other state-of-the-art similar forgery detection methods.

Keywords: image forgery detection; Weber local descriptor; local binary pattern; splicing forgery; copy-move forgery; multi-scale method.

1. Introduction

Nowadays, we are living in an age, where digital imaging has grown and developed to become the widespread technology. It plays a significant role in human life, where the digital images are currently considered a rich means of capturing pictorial information, which is being used in daily newspapers, magazines, military, and may be used as an evidence in court of law or in medical diagnose field [1]. With the increasing applications of digital imaging, different types of software have been introduced for image processing. Such software can do an alteration in a digital image by changing regions of an image or combining two images without leaving noticeable effects of the modification in the forged image. These modifications cannot be noticed by human eyes. The image forgeries can wipe off an important object from a proof image, which can be used to mislead the court of law. Therefore, the security of digital images is a very serious topic of research. The most commonly used forgery is copy-move forgery (CMF), where a region is copied and pasted to another place in the same image in order to conceal an important object from the original image. The copied block may be changed by some pre-processing operation such as rotation, scaling, additive noise, etc. to match the copied area with the whole image. In another similar type of forgery, one part of an image is copied and pasted to another image. This type of forgery is known as image splicing. The detection of these two types of forgeries is the subject of this paper.

Many techniques have been developed for validating the authenticity of digital images. These techniques can be broadly divided into intrusive (active) and non-intrusive (blind or passive) techniques [2]. The intrusive techniques can further be classified into two categories: (1) those that embed a watermark in an image and (2) digital signature-based techniques. In these methods, particular information is embedded in digital images for supporting multimedia digital authentication and rights safety. Once the image contents are modified, the embedded information will also be altered. The image authenticity is verified by checking whether the true signature matches the signature that is retrieved from the suspicious test image. These techniques are restricted because of the inability of many digital cameras to embed the signature. Due to the restrictions of active techniques, the researchers tend to develop non-intrusive techniques for validating the authenticity of digital images. These techniques examine images without the assumption of embedded information such as signatures or watermarks.

Different approaches have been adopted for non-intrusive image forgery detection [2, 16]. The techniques based on supervised learning use specific features to discriminate the forged image from authentic ones. These techniques have been fairly successful in identifying whether an image is original or forged, but the number of false positives/negatives is high. Assuming that forgery disturbs the texture micro-patterns of

an image, we employed texture descriptors to encode the structural changes in an image caused by forgery. We employed multi-WLD descriptor, which is one of the best stat-of-the-art descriptors, and got promising results for copy-move and splicing forgery detection [25, 26]. This paper extends the previous work [27, 28] on the multi-WLD. Optimal parameter values are obtained. These optimum values are used with the multi-WLD on three data sets. These results are thoroughly compared with the multi-LBP. Extensive analysis with various scale combinations indicates the multi-WLD outperforms.

The forgery can be either copy-move or spliced. Multi-WLD and multi-LBP features are extracted from the chrominance components of a color image. Feature selection is applied to reduce the dimension of the feature space and to get rid of redundant features. SVM is used for classification purpose. The forgery detection method based on multi-WLD has been evaluated on three publicly available benchmark data sets (CASIA v1.0, CASIA v2.0, and Columbia color) developed for forgery detection. The method based on multi-LBP has been evaluated only on CASIA v1.0 data set; we tested different variants of LBP. A comparison between multi-WLD and multi-LBP descriptors has been given. We found that multi-WLD based forgery detection method not only outperforms multi-LBP based method, but it also achieved high detection rate on the three benchmark data sets as compared to state-of-the-art methods.

The rest of the paper is organized as follows. Section 2 review some related work while Section 3 presents the detail of image forgery detection methods. Section 4 deals with experimental setup. Section 5 describes the detection performance with multi-WLD while Section 6 presents the detection performance with multi-LBP. Section 7 discusses the results. Section 8 gives a comparison with other methods, and finally Section 9 draws the conclusion.

2. Related Work

Non-intrusive image forensics is focused on developing technologies to decide about a suspicious image, whether it is authentic or tampered without assuming any embedded watermark or digital signatures. This area attracted the attention of some researchers during the past few years, and many techniques for digital image forgery detection have been introduced. In the following paragraphs, we give just an overview of some related methods. For detail, an interested is referred to [2, 16].

An improved DCT (discrete cosine transform)-based technique was proposed to discover CMF in digital images [3]. In this method, first an image is subdivided into blocks, and DCT is computed. Then the DCT coefficients are lexicographically sorted and used to compare different blocks. This technique is robust against JPEG compression, additive white Gaussian noise and blurring distortion. Cao et al. [4] proposed another technique based on improved DCT for locating the duplicated regions in a given image. This method uses circular blocks for representing the image applying DCT coefficient.

Muhammad et al. [5] proposed an image forgery detection method that is based on noise pattern. In this method, first noise pattern is obtained by subtracting the denoised image from the input image. Then, histograms of noise from different segments of the image are compared to find the distortion caused by image forgery. Peng et al. [6] used sensor noise pattern for detecting image forgery. Instead of employing the histogram, they used four statistical measures namely, variance, entropy, signal-to-noise ratio, and average energy gradient calculated from the noise pattern.

He et al. [7] proposed a method that relies on approximate run length (ARL) to detect CMF. First, the edge-gradient array of a given image is calculated, and then ARL is computed along edge-gradient orientations. Zhao et al. [8] used chrominance spaces with RLRN (run-length run-number) for CMF detection. First, the input color image is transformed into YCbCr color space. Then RLRN is used to extract the features from the de-correlation of chrominance components. SVM is used for classification purpose. This method gives better performance with JPEG images than TIFF images.

Undecimated wavelet transform (UWT) based image forgery detection method was proposed in [9]. Approximation and detailed coefficients from UWT decompositions of overlapping blocks of an image are used to find the similarity between the blocks. The method is robust against JPEG compression and a certain degree of rotation and scaling.

Scale invariant feature transform (SIFT) based forgery detection methods were proposed in [10-12]. They are quite robust against rotation and scaling post-processing.

Shi et al. [13] proposed statistical features based on 1D and 2D moments, and transition probability features based on Markov chain in DCT domain for image splicing detection [13]. On the CASIA v2.0 database [14], the method achieved 84.86% accuracy. Later, He et al. [15] improved the method by combining transition probability features in DCT and DWT domains. For classification, they used SVM together with recursive feature elimination (RFE). Their method obtained 89.76% accuracy on the CASIA v2.0 database.

Most of the non-intrusive techniques, which have been proposed so far, face many challenges such as doing more robust fully automatic forgery detection, reducing the rate of false positives/negatives, robustness for tamper detection in any kind of image format, etc. In this research, our focus is on reducing the number of false positives/negatives and robustness against any kind of image format.

3. Image Forgery Detection System

In this section, we give an overview of the Image Forgery Detection System that was initially proposed in [25]. Figure 1 shows a block diagram of this system. The first step is preprocessing; input color image is converted from RGB space into YCbCr space. The second step is feature extraction where a chrominance component (either Cb or Cr) is used to extract texture features employing multi- WLD and multi-LBP. LLB algorithm [19] for feature subset selection is used to eliminate irrelevant features for decreasing the complexity of the system. In the last step, SVM is used to identify an input image as authentic or forged.

3.1. Preprocessing (Conversion from RGB to YCbCr Space)

Image forgers generally do image tampering in RGB space and attempt to wrap manipulated traces. As human eyes are less sensitive to chrominance components of YCbCr space, so the tapering traces are filtered into chrominance components. As such for detecting copy-move or splicing forgery in a digital image, chrominance components are more effective [8]. Keeping in view this observation, first the input color image is transformed into YCbCr space. The chrominance components are computed by subtracting luminance component from red (Cr = R-Y) and blue (Cb = B-Y). The transformation from RGB to YCbCr space is given below:

$$Y = 0.299\,R + 0.587\,G + 0.114\,B \quad (1)$$

$$Cr = 0.701\,R - 0.587\,G - 0.114\,B \quad (2)$$

$$Cb = -0.299\,R - 0.587\,G + 0.886\,B. \quad (3)$$

YCbCr space stores the color information in terms of luminance and chrominance components. Figure 2 shows an image in RGB space and the component images in YCbCr space.

3.2. *Feature extraction*

For a robust forgery detection system, it is very important how the tampering traces are molded. The accuracy of the system is based mainly on this modeling. We assume that tampering disturbs the texture patterns in an image, and this change can be modeled using texture descriptors. For this purpose, we employ two stat-of-the-art texture descriptors: multi-scale WLD and multi-scale LBP. In the following subsections, we give an overview of these descriptors.

3.2.1. *Multi-scale WLD* (*multi-WLD*)

WLD is a robust local descriptor, which is based on Weber's law, which quantifies the fact that human sensitivity of a sample relies on the change of the original stimulus intensity [17]. WLD is a local texture descriptor. It has many interesting characteristics such as edge detection and robustness against illumination and noise changes. It has two components: differential excitation (D) and orientation (Φ).

According to Weber's law, the ratio of the increment threshold to the intensity of the background is a constant, which is formulated as follows:

$$\frac{\Delta x}{x} = C, \quad (4)$$

where x is the background intensity, Δx is the increment threshold (noticeable distinction), and C is a constant. This formula is used to compute differential excitation (D). The $D(p_c)$ of a pixel p_c is calculated using the filter f_{00} (shown in Figure. 3) as follows:

$$D(p_c) = arctan\left[\sum_{i=0}^{N-1}\left(\frac{p_i - p_c}{p_c}\right)\right] \quad (5)$$

where p_i is the i^{th} neighbor of pixel p_c and N is the total number of neighbors.

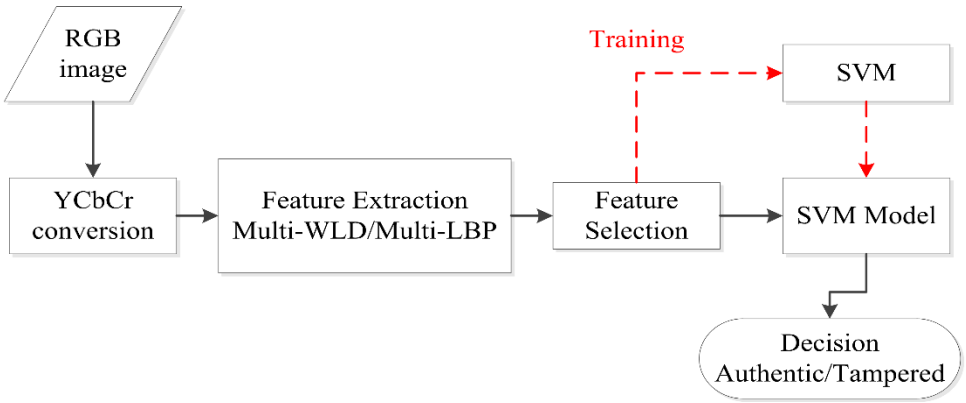

Figure 1. Diagram of the image forgery detection method based on texture descriptors.

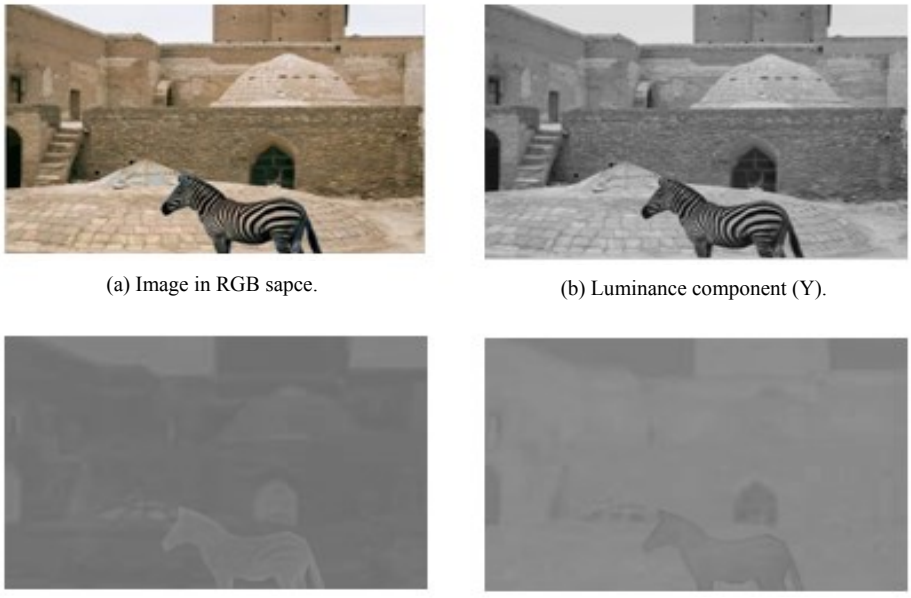

(a) Image in RGB sapce.

(b) Luminance component (Y).

(c) Chrominance component (Cb).

(d) Chrominance component (Cr).

Figure 2. Image in RGB space and corresponding luminance and chrominance components.

WLD orientation component Φ is the gradient orientation. For pixel p_c, it is calculated as follows:

$$\Phi(p_c) = arctan\left(\frac{k_S^{11}}{k_S^{10}}\right) \quad (6)$$

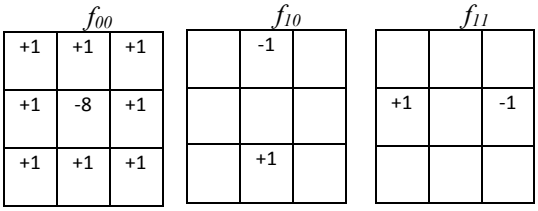

Figure 3. Filters used in simple WLD calculation

where, k_s^{11} and k_s^{10} are the outputs of the filters f_{11} and f_{10} (shown in Figure 3), respectively.

The range of Φ is $[-\pi, \pi]$, first it is mapped to Φ' whose range is $[0, 2\pi]$ and then it is quantized into T dominant orientations.

After calculating differential excitation and gradient orientation, WLD histogram is calculated using D and Φ', the detail can be found in [17]. The computation of WLD histogram involves three parameters: the number of dominant orientations (T), the number of differential excitation segments (M), and the number of bins in each differential excitation segment. Simple WLD descriptor uses 3x3 neighborhood about the central pixel. It is not capable of capturing the detail of all local texture micro-patterns, which exist with different scales. Multi-WLD can capture the detail of texture micro-patterns with different scales and it is computed using symmetric square neighborhoods (P, R) with varying P (the number of neighboring pixels) and R (the radius that represents scale). For multi-WLD, we employed three neighborhoods: (8, 1), (16, 2), and (24, 3). Figure 4 shows f_{00} filters for (16, 2) and (24, 3) scales. The histograms computed with three neighborhoods are concatenated to produce the multi-WLD that forms the representation of the image. Figure 5 shows WLD histograms of a tampered image with three scales. Figure 6 shows histograms of multi-WLD (after concatenation of histograms with three neighborhoods) of Cr component of an authentic image and a spliced image. The multi-WLD histograms of Cr component of authentic image and the corresponding copy-move forged image without doing any preprocessing on the copied region are illustrated in Figure 7. Multi-WLD histograms of Cr component of an authentic image and the corresponding copy-move image forged with performing a rotation on the copied region are shown in Figure 8.

3.2.2. *Multi-scale LBP (Multi-LBP)*

LBP has been confirmed to be a very effective local texture descriptor. It encodes local texture micro-patterns and has been successful in many fields. LBP offers a unified description comprising both structural and statistical characteristics of texture patterns, thus it is robust for texture analysis. LBP descriptor has low computational cost and is robust against monotonic illumination changes. An LBP operator associates a binary code with each pixel p taking into account its N neighborhood pixels located on a circle of radius R. Formally, it is defined as follows:

$$LBP_{N,R} = \sum_{n=0}^{N-1} s(p_n - p_c)2^n \tag{7}$$

1	1	1	1	1
1	0	0	0	1
1	0	-16	0	1
1	0	0	0	1
1	1	1	1	1

a) f_{00} filter of (16,2) scale

1	1	1	1	1	1	1
1	0	0	0	0	0	1
1	0	0	0	0	0	1
1	0	0	-24	0	0	1
1	0	0	0	0	0	1
1	0	0	0	0	0	1
1	1	1	1	1	1	1

b) f_{00} filter of (24,3) scale

Fig. 4. f_{00} filters for (16,2) and (24,3) scales.

a) Tampered Image

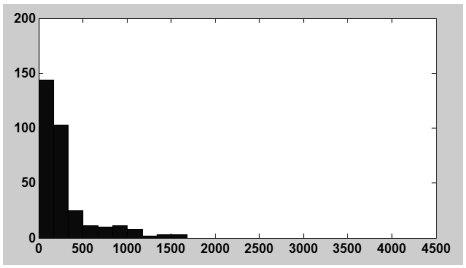

b) WLD histogram with (8, 1) scale

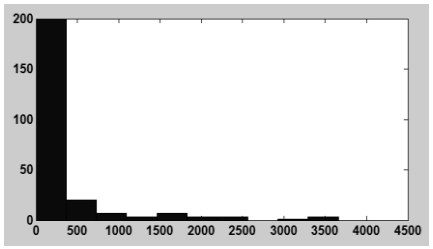

c) WLD histogram with (16, 2) scale

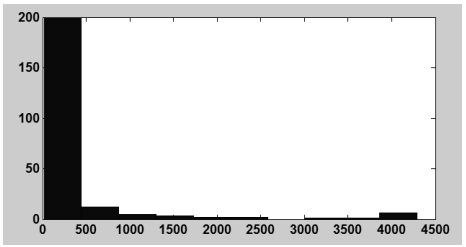

d) WLD histogram with (24, 3) scale

Fig. 5. WLD histograms of a tampered image with three scales.

where the thresholding function s(x) is specified as follows:

$$s(p_n - p_c) = \begin{cases} 1 & p_n - p_c \geq 0 \\ 0 & p_n - p_c < 0. \end{cases} \quad (8)$$

Here p_c is the grayscale value of pixel p_c and p_n (n= *0, 1, ..., N-1*) are the gray-scale values of its neighbors.

There are three variants of LBP operator: (1) rotation invariant LBP denoted by $LBP_{N,R}^{ri}$, (2) uniform LBP denoted by $LBP_{N,R}^{u2}$, and (3) uniform rotation-invariant LBP denoted by $LBP_{N,R}^{riu2}$ [18]. The rotation invariant LBP is computed using the following equation:

$$LBP_{N,R}^{ri} = min\{ROR(LBP_{N,R}, i) | \, i = 0,1, \dots, N-1\} \quad (9)$$

Simple LBP operator considers only 3×3 neighborhood of a pixel for computing its LBP code. Similarly to WLD, LBP cannot encode texture micro-patterns at multiple scales. Like multi-WLD, multi-LBP is defined using multiple neighborhoods (P, R) of varying P (the number of neighboring pixels) and R (the radius that defines scale). In our experiments, we employed three scales: P = 8, 12, 16 and R = 1, 1.5, 2.

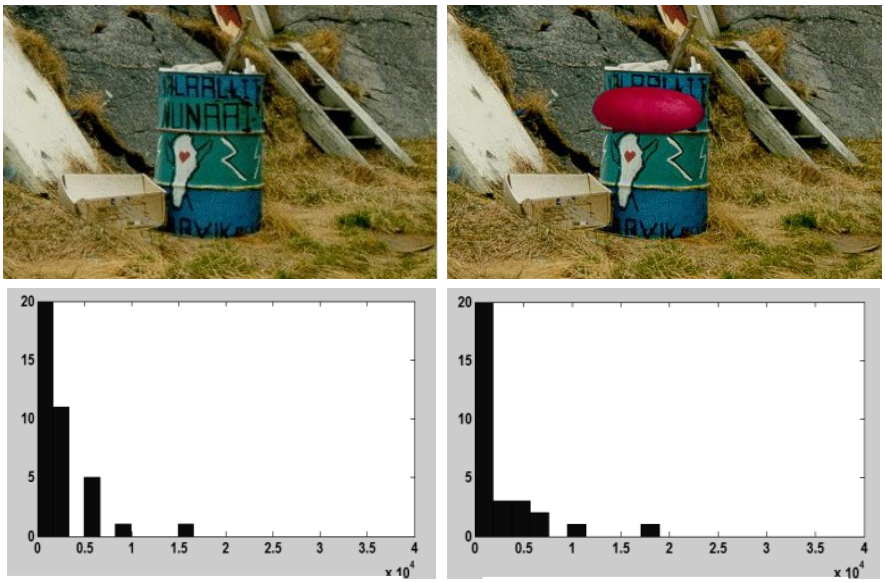

Multi-scale WLD histogram bins of authentic image

Multi-scale WLD histogram bins of forged image

Fig. 6. Multi-WLD histograms of Cr chrominance component of an authentic image (left) and a spliced image (right).

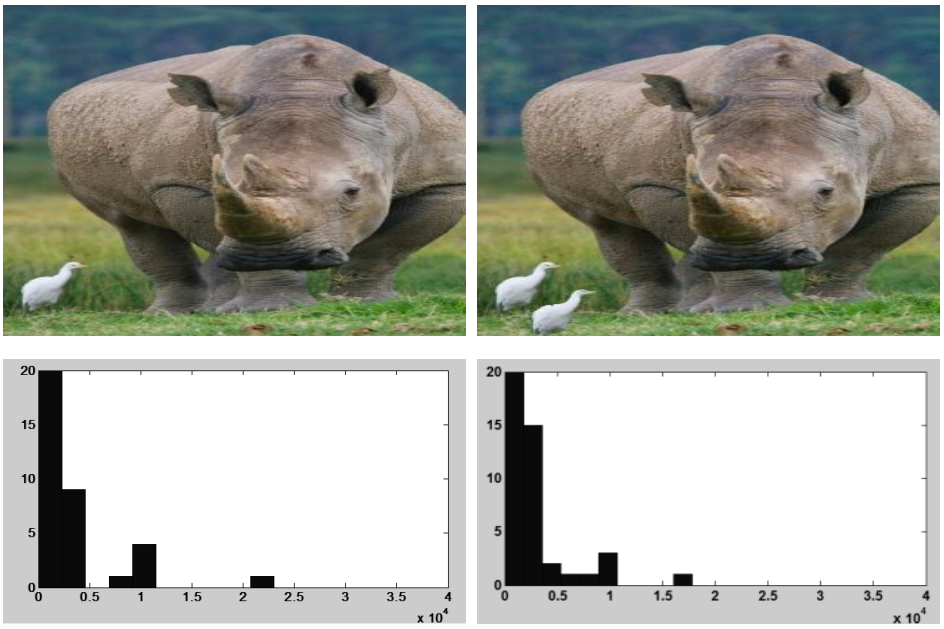

Multi-WLD histogram of authentic image

Multi-WLD histogram of forged image

Fig. 7. Multi-WLD histograms of Cr component of an authentic image (left) and a copy-move image (right) forged without any preprocessing on the copied region.

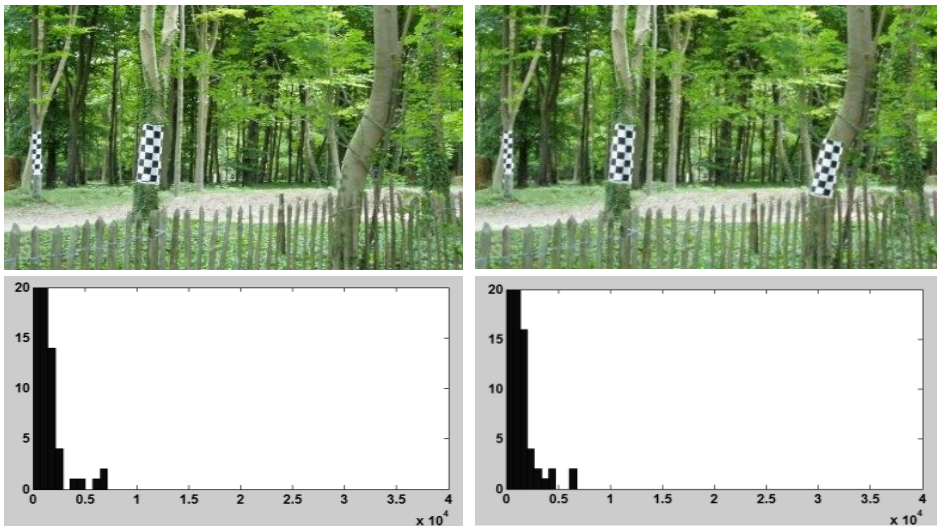

Fig. 8. Multi-WLD histograms of Cr component of an authentic image (left) and a copy-move image (right) forged with performing rotation on the copied region.

3.3. *Feature Subset Selection*

Each of multi-WLD and multi-LBP descriptor contains a lot of redundant features, which not only causes the curse of the dimensionality problem but also tends to reduce the performance accuracy of a classifier. Local learning based (LLB) feature subset selection method [19] is computationally efficient and is not sensitive to the large number of irrelevant features. The main design of this algorithm is to decompose randomly a complicated non-linear problem into a group of locally linear problems by using local learning, and then to learn feature relevance globally in the maximum margin framework. Though LLB is a filter method for feature subset selection, but we use it as a rapper method with SVM.

3.4. *Classification*

To identify an image as authentic or tempered is a two-class classification problem and for this purpose, we employed SVM, which has better generalization. SVM is modeled using training patterns (x_i, y_i), $i = 1, 2, \ldots, M$, where $x_i \in R^d$ and is a feature vector, $y_i \in \{-1,+1\}$ and is a class label, -1 and $+1$ label authentic and tampered images, respectively. SVM modeling process builds an optimal hyper-plane with maximum margin that ensures better generalization performance. The margin is defined as the distance between the nearest data points of each class and the hyper-plane [20]. Basically, SVM is a linear classifier but usually the samples of two classes are not linearly separable, to overcome this problem kernel trick is used that transforms the original space to a higher-dimensional space, where the problem becomes linear, using a kernel function. Different choices for kernel functions are possible, but the most commonly

used kernels are RBF and polynomial kernels, which have performed well in most of the application. RBF and polynomial kernels are employed in the experiments of the paper.

4. Experimental Setup

In this section, we describe the datasets, the evaluation policy and performance measures that were used for the performance evaluation of our method.

4.1. *Datasets*

The proposed method was evaluated on three benchmark datasets that are designed for image forgery detection. The three databases are CASIA TIDE v1.0 and v2.0 [14], and Columbia authentic and spliced color image dataset [23].

CASIA v1.0 dataset was released in January 2010. It consists of two sets of images: 800 authentic images and 921 tampered images. All images have 384×256 sizes and they are in JPEG format. The original images are categorized into eight groups: animal, scene, character, plant, nature, architecture, texture and article. The authentic images from every group were arbitrarily chosen to create the tampered images. The tampering was done by copy-and-paste process; in some cases geometric transformations such as rotation, resizing were applied on copied regions before pasting. The tool used to generate the tampered images was Adobe Photoshop. Out of 921 forged images, 459 are copy-move forged and the remaining are spliced.

CASIA v2.0 dataset consists of 7491 authentic and 5123 forged images, which are in JPEG, BMP, and TIFF formats and the image sizes vary from 240×160 to 900×600 pixels. For some forged images, scaling and rotation operations have been applied on copied regions before pasting.

Columbia color image dataset consists of 183 authentic and 180 spliced images, which are in TIFF format. The image size is 1152×768. The spliced images were created using the authentic images, without any pre-processing.

4.2. *Evaluation policy*

The feature descriptors, feature subset selection method and the classifier involve free parameters, which need tuning for optimal performance.

Three scales (8, 1), (16, 2) and (24, 3) of multi-WLD can be combined in different ways to get the scales from C1 to C7, where C1 means (8, 1), C2 corresponds to (16, 2), C3 refers to (24, 3), C4 is a combination of (8, 1) and (16, 2), C5 is a combination of (8, 1) and (24,3), C6 is a combination of (16, 2) and (24, 3), and finally, C7 is the combination of all the scales (8, 1), (16, 2) and (24, 3). We examined all these scales to find the one that gives best performance. In addition, multi-WLD has three parameters (T, M, S), various combinations of these parameters were tried to see the effects of these parameters on the detection accuracy.

Similarly to multi-WLD, the three scale of multi-LBP were combined in different ways to from the scales from C1 to C7, where C1 means (8, 1), C2 corresponds to (12, 1.5), C3 refers to (16, 2), C4 is a combination of (8, 1) and (12, 1.5), C5 is a combination of (8, 1) and (16,2), C6 is a combination of (12, 1.5) and (16, 2), and finally, C7 is the

combination of all the scales (8, 1), (12, 1.5) and (16,2). There are four variants of LBP, we performed experiments will all to find out which variant gives the best performance.

SVM classifier with RBF and polynomial has also free parameters. We used grid search method with 5-fold cross validation to find the optimal values of these parameters. The optimal parameter values for RBF kernel are $C = 2^{16}$ and $g = 2^{-14}$, while those for polynomial kernel are $C = 2^{-3}$, $g = 2^{-3}$, cf = 10, and d = 2. LIBSVM was utilized for SVM implementation [24].

To evaluate the forgery detection system, we employed 10-fold cross validation and used the performance measures of true negative rate (*TNR*), true positive rate (*TPR*), accuracy (*ACC*) and area under ROC curve (*AUC*). TPR is a measure of classification accuracy of true cases and it is calculated as

$$TPR = (100 * TP / (TP + FN)) \tag{10}$$

TNR is a measure of classification accuracy of false cases and it is calculated as

$$TNR = (100 * TN / (FP + TN)) \tag{11}$$

Accuracy is percent ratio between correctly classified images over total number of images and is expressed as

$$ACC = 100 * (TP + TN) / (TP + TN + FN + FP) \tag{12}$$

where *TP* (true positive) is the number of tampered images which were classified as tampered images, *FN* (false negative) is the number of tampered images misclassified as authentic images, *FP* (false positive) is the number of authentic images misclassified as tampered images, and *TN* (true negative) is the number of authentic images, which are correctly classified as authentic images.

The value of *AUC* is between 0 and 1 and calculating using ROC curve.

5. Detection Performance with Multi-WLD

In this section, we present the detection results with multi-WLD in detail on three datasets and discuss its impact on various factors related to the copied region.

5.1. *Experiments with CASIA v1.0*

First we discuss the tuning of multi-WLD parameters, described in Section 4.2. For experiments with CASIA v1.0 dataset, we considered three experiment cases: splicing detection, copy-move detection and forgery detection (splicing + copy-move). Then we present results for the detection of splicing and copy-move forgeries, and finally discuss the impact of various factors related to copied region.

5.1.1. *Parameter tuning*

First we discuss the effect of T, M, S parameters of multi-WLD. Figure 9 shows the effects of these parameters with C7 scale and Cr component, the effects with Cb are similar; these results are without feature selection. These results indicate that the best accuracy is achieved when T = 4, M = 4 and S = 20. For the results given in the following sections, we use only these parameter values.

The effects of multi-WLD scales C1-C7 are shown in Figure 10 for forgery detection (splicing + copy-move) with Cr component; these results are obtained with the parameters: T = 4, M = 4, and S = 20, LLB feature subset selection and SVM using polynomial kernel. Out of individual scales (C1, C2, C3), C3 gave the best performance, but overall scale C7 (the combination of C1, C2, C3) resulted in the highest detection

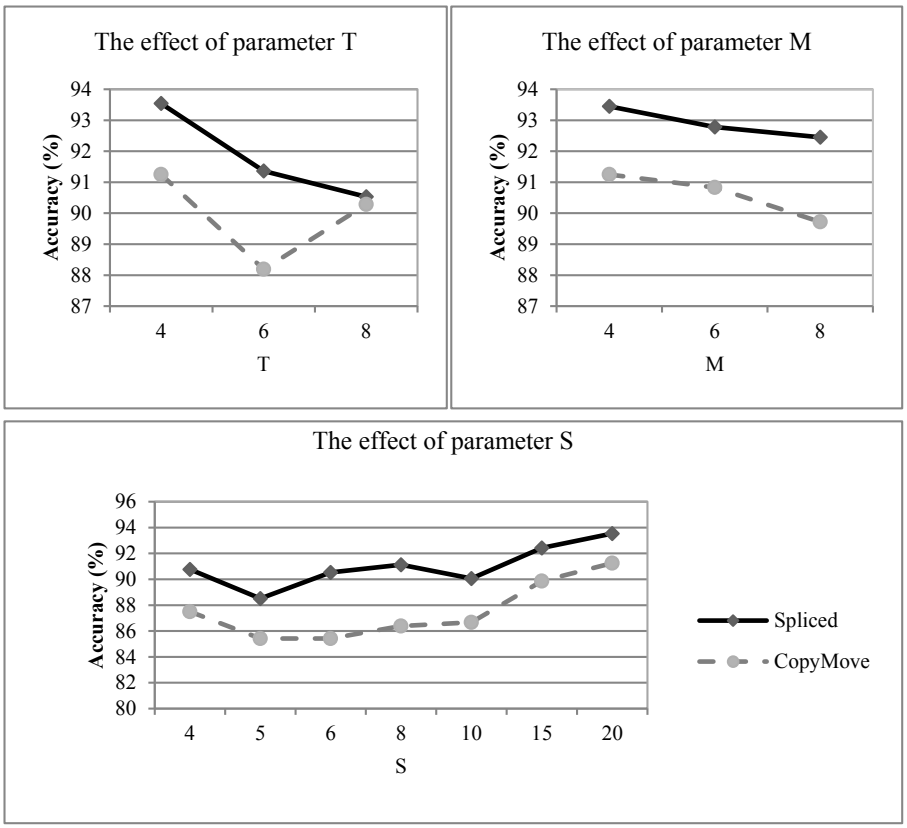

Fig. 9. Effects of T, M, S parameters on forgery detection with Cr chrominance component and C7 scale.

accuracy. The scale C7 achieved accuracies of 92.62% and 88.66% with Cr and Cb components, respectively. It experimentally proves that multi-WLD performs better than individual single WLD scales in case of image forgery detection. Each single WLD scale produces 320 features (bins in the histogram), and C7 has a total of (320×3=) 960 features. All the subsequent results are with C7.

In the next experiment, Cr and Cb histograms were fused and we call it feature level fusion (FLF), in this case the feature vector is of dimension 1920 (=960×2), which is reduced to 770 features after feature subset selection. FLF performs better than individual chrominance components, it achieved 94.19% accuracy for full CASIA v1.0 dataset (splicing + copy-move) with SVM using polynomial kernel. False positive rate and false negative rate are 6.3 and 3.7, respectively.

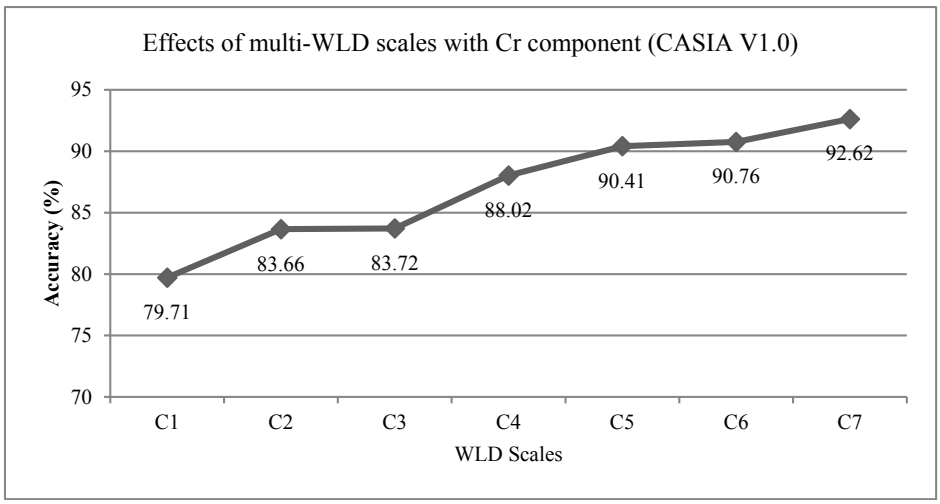

Fig. 10. The accuracy of image forgery detection with multi-WLD scales C1-C7 and Cr component.

Further to examine the effect of kernel on the performance of SVM, we performed experiments with RBF and polynomial kernels. Table 1 gives a comparison between polynomial and RBF kernels when FLF system is used. Polynomial kernel performed better than RBF kernel in our experiments, so we report results only with polynomial kernel in the following experiments.

Table 1. The performance comparison between RBF and polynomial kernels on CASIA v1.0 with FLF.

Kernel	ACC(%)±Std	AUC± Std	FP	FN	#Features
Poly	**94.19 ± 1.60**	0.942 ± 0.022	6.3	3.7	770
RBF	92.50 ± 2.20	0.930 ± 0.030	7.7	5.2	923

Table 2. Performance of different channels with C7 scale of WLD in splicing detection.

Channel	ACC(%)±Std	AUC± Std	TPR(%)	TNR(%)
Cr	94.29±2.50	0.94±0.02	94.80	93.44
Cb	90.60±3.82	0.91±0.04	92.25	89.53
FLF(Cr+Cb)	94.52±1.84	0.94±0.02	95.05	93.86
Y	54.64±4.02	0.50±0.09	98.91	2.52

5.1.2. *Results on Splicing Detection*

Using the optimal parameters as discussed in Section 5.1.1, we performed experiments for splicing detection with individual chrominance component, their fusion and luminance component; the results are shown in Table 2. The Cr component and FLF both gave comparable results in terms of AUC but FLF performed slightly better in terms

accuracy, TPR and TNR. Luminance component resulted in the worst detection performance.

5.1.3. *Results on copy-move forgery detection*

For copy-move forgery detection, the results are shown in Table 3 with individual chrominance component, their fusion, and luminance component; for experiments we employed the optimal parameters discussed in Section 5.1.1. In this case, the Cr component gave an accuracy of 91.11±3.35, which is better than those obtained by Cb, FLF and Y but in terms of AUC, TPR and TNR, ELF performed slightly better than Cr. The performance of luminance component Y is poor also for copy-move detection.

Table 3. Performance of different components with multi-WLD on copy-move detection.

Channel	ACC(%)±Std	AUC± Std	TPR(%)	TNR(%)
Cr	91.11±3.35	0.88±0.05	95.43	83.64
Cb	87.22±3.19	0.85±0.04	95.23	77.92
FLF(Cr+Cb)	90.97±2.72	0.90±0.05	96.73	83.90
Y	68.33±5.09	0.59±0.08	93.43	24.35

If we compare Table 2 and Table 3, we find that copy-move forgery detection has lower accuracy (90.97%) than splice detection accuracy (94.52%) with FLF system. This can be attributed to the fact that in copy-move forgery, the hidden noise pattern remains almost same, while in splicing there are two different background patterns as they come from two different images. This indicates that it is comparatively easier to detect splicing than copy-move forgery.

5.1.4. *Results on Forgery Detection* (*Splicing + Copy-move*)

Results for forgery detection are shown in Table 4 with multi-WLD (C7). The chrominance components (Cb and Cr) gave better accuracies than the luminance component (Y). When the chrominance components were fused (FLF case), the accuracy increased to 94.19%. In terms of AUC, TPR and TNR, FLF gave better detection performance. Figure 11 shows ROC curves of chrominance components and FLF.

A comparison of the effect of multi-WLD for splicing, copy-move and forgery detection with Cr, Cb and FLF is given in Figure 12. The performance of multi-WLD is better for splicing and forgery (splicing+copy-move) detection than copy-move detection. Overall, FLF stands first in the detection accuracy, Cr is its close competitor for splicing detection. The overall performance of Cb is poor.

Table 4. Performance of different components with multi-WLD for forgery detection.

Channel	ACC(%)±Std	AUC±Std	TPR(%)	TNR(%)
Cr	92.62 ± 2.26	0.93 ± 0.02	94.45	90.45
Cb	88.66 ± 2.49	0.88 ± 0.03	91.46	85.44
FLF(Cr+Cb)	**94.19 ± 1.60**	0.94 ± 0.02	96.02	92.05
Y	61.80± 2.85	0.61± 0.04	67.71	55.27

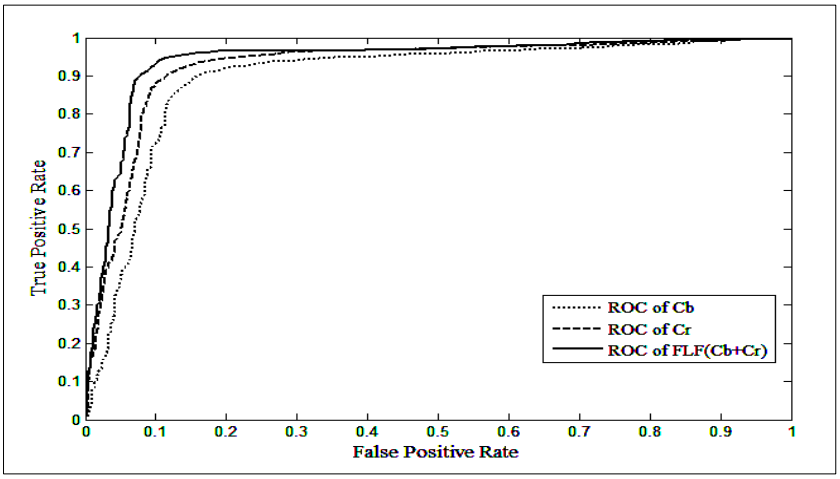

Fig. 11. ROC curves for forgery detection with multi-WLD on CASIA v1.0.

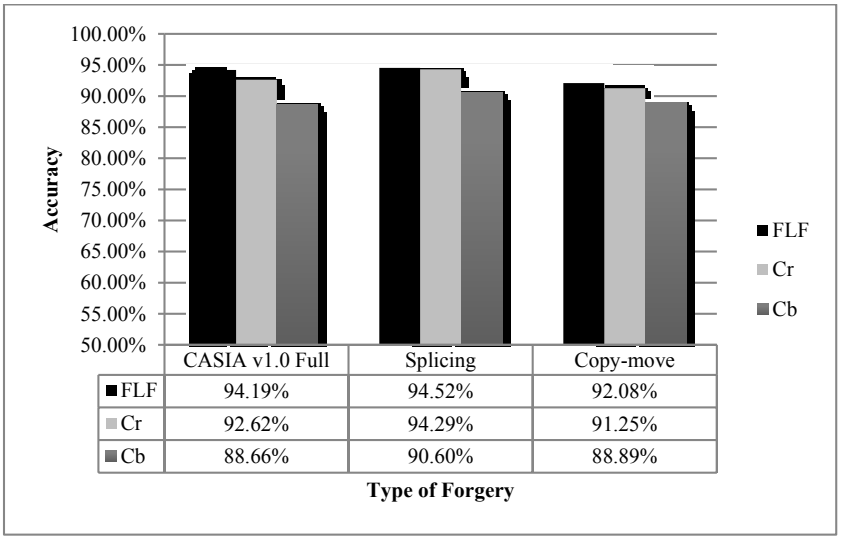

	CASIA v1.0 Full	Splicing	Copy-move
FLF	94.19%	94.52%	92.08%
Cr	92.62%	94.29%	91.25%
Cb	88.66%	90.60%	88.89%

Fig. 12. Accuracy of the detection method using multi-WLD on CASIA v1.0.

5.1.5. *The impact of multi-WLD on forgery detection with transformation*

Sometimes the copied region is pasted after applying some transformation such as rotation, scaling and deformation. We performed experiments to examine how much multi-WLD is robust against these transformations. Table 5 illustrates the results for splicing detection. There are three common types of transformation: (a) deform, (b) resize and (c) rotate the copied region before pasting. Column 2 of Table 5 shows the number of authentic (Au) and forged (Fg) images that fall into the corresponding transformation

category in the data set. From the table, we find that rotation gives the least accuracy of 88.57%, while deform gives the best accuracy of 95%. However, this trend might be related to the number of images in the category, for the case of rotation, the number of images is small.

Table 6 gives the results for copy-move detection for the case transformation. The highest accuracy of 90.82% was achieved with no transformation. The results are not conclusive in this case because the number of samples is very small, which is not enough to properly train SVM.

Table 5. Performance for splicing detection involving transformation with multi-WLD

Type	#images (Au / Fg)	Component	ACC(%)± Std	AUC± Std
Deform	39 / 41	Cr	91.25± 15.65	0.93±0.11
		Cb	78.75± 14.49	0.79±0.20
		FLF	**95.00± 6.45**	**0.93±0.12**
Resize	183 / 165	Cr	**92.06± 5.20**	**0.92±0.05**
		Cb	88.82± 4.96	0.91±0.06
		FLF	91.47± 4.48	0.91±0.05
Rotate	18 / 18	Cr	88.57± 11.95	0.86±0.13
		Cb	82.85± 15.65	0.76±0.22
		FLF	**88.57± 11.95**	**0.93±0.07**
No transformation	156 / 152	Cr	92.00± 5.26	0.95±0.03
		Cb	88.00± 6.70	0.89±0.08
		FLF	**93.00± 6.93**	**0.93±0.07**

Table 6. Performance for copy-move detection involving transformation with multi-WLD

Type	#images (Au / Fg)	Component	Acc(%)± Std	AUC± Std
Deform	12/12	Cr	**90.00 ± 13.69**	**0.95±0.11**
		Cb	80.00 ± 11.18	0.83±0.24
		FLF	80.00 ± 20.92	0.83±0.24
Resize	23/23	Cr	75.56 ± 14.49	0.71±0.16
		Cb	68.89 ± 14.49	0.68±0.12
		FLF	**75.56 ± 4.97**	**0.75±0.11**
Rotate	7 /7	Cr	90.00 ± 22.36	-
		Cb	70.00 ± 27.39	-
		FLF	**90.00 ± 22.36**	-
No transformation	406 / 204	Cr	**90.98 ± 4.84**	**0.90±0.05**
		Cb	88.20 ± 2.42	0.84±0.04
		FLF	90.82 ± 2.39	0.90±0.07

5.1.6. *The impact of multi-WLD on the shape of the tampered region*

The tampered region can be of different shapes and can put difficulty for detection. CASIA v1.0 involves three shapes of the tampered region: (a) rectangular, (b) circular and (c) arbitrary or irregular. Table 7 and Table 8 give the detection performance for

splicing and copy-move, respectively, of multi-WLD when the database has been grouped based on the shape of tampered region. In the case of splicing detection, 94.43% accuracy was obtained with arbitrary shape, while 90% and 85% accuracies are achieved with circular and rectangular shapes, respectively. In the case of copy-move forgery detection, Cr performs better than the combined chrominance channels in most of the shape cases.

Table7. Performance for splicing detection with multi-WLD based on the shape of tampered region

Type	#images (Au / Fg)	Component	ACC(%)±Std	AUC±Std
Arbitrary	325 / 372	Cr	92.41±2.98	0.92±0.03
		Cb	90.25±2.67	0.90±0.03
		FLF	94.43±2.08	0.95±0.03
Circular	12 / 12	Cr	90±13.69	0.87±0.18
		Cb	85±13.69	0.88±0.16
		FLF	90±13.69	0.90±0.22
Rectangular	21 / 21	Cr	82.5±11.18	0.82±0.19
		Cb	70±6.85	0.70±0.11
		FLF	85±5.59	0.90±0.09

Table 8. Performance for copy-move detection with multi-WLD based on the shape of tampered region

Type	#images (Au / Fg)	Component	ACC(%)±Std	AUC±Std
Arbitrary	111 / 110	Cr	88.18±6.14	0.89±0.06
		Cb	88.64±7.50	0.90±0.08
		FLF	87.27±7.96	0.88±0.09
Circular	102 / 102	Cr	83.00±8.56	0.81±0.11
		Cb	75.00±7.45	0.75±0.13
		FLF	77.00±10.06	0.79±0.11
Rectangular	148 / 148	Cr	82.41±6.59	0.79±0.09
		Cb	75.17±10.38	0.77±0.09
		FLF	79.66±10.08	0.80±0.11
Triangular	101 / 101	Cr	79±8.10	0.79±0.10
		Cb	77.5±5.89	0.79±0.08
		FLF	75±9.13	0.75±0.12

5.1.7. *The impact of multi-WLD on the size of the tampered region*

The spliced and copy-move images are split into three groups based on the size of the tampered region: (a) large tampered region, (b) medium tampered region and (c) small tampered region. The reported results in Tables 9 and 10 are based on this categorization and SVM with RBF kernel. In the case of splicing detection, multi-WLD with Cr component gives better accuracy whatever the size of the tampered region. The accuracy is 93.0% for the large tampered region but it is 91% with medium and small size of the tampered region. In the case of copy-move forgery detection, the accuracy is 86.67% with feature level fusion when the size of the tampered region is large. These results

indicate that the size of the tampered region has impact on the detection accuracy, which is less in case of splicing as compared to copy-move forgery.

Table 9. Performance for splicing detection with multi-WLD based on the size of tampered region

Type	#images (Au / Fg)	Component	ACC(%)±Std	AUC±Std
Large	50/50	Cr	93.0±8.23	0.94±0.10
		Cb	91.0±9.94	0.92±0.11
		FLF	92.0±10.33	0.91±0.14
Medium	50/50	Cr	91.0±7.38	0.92±0.12
		Cb	89.0±9.94	0.92±0.09
		FLF	90.0±9.43	0.94±0.10
Small	50/50	Cr	91.0±8.76	0.92±0.12
		Cb	78.0±14.76	0.86±0.13
		FLF	87.0±4.83	0.88±0.08

Table 10. Performance for copy-move detection with multi-WLD based on the size of tampered region

Type	#images (Au / Fg)	Component	ACC(%)±Std	AUC±Std
Large	30/30	Cr	81.67±18.34	0.80±0.28
		Cb	80.00±20.49	0.77±0.30
		FLF	86.67±15.32	0.89±0.14
Medium	30/30	Cr	81.67±16.57	0.85±0.22
		Cb	75.00±16.20	0.73±0.22
		FLF	75.0±19.64	0.81±0.24
Small	30/30	Cr	81.67±14.59	0.79±0.18
		Cb	81.67±16.57	0.76±0.26
		FLF	80.00±15.32	0.85±0.23

5.2. *Experiments with CASIA v2.0*

We did through analysis of the impact of multi-WLD on the forgery detection using CASIA v1.0, which gives the idea of the strengths and weakness of multi-WLD keeping in view different factors. CASIA v1.0 is relatively small database and all images are in JPEG format. To further investigate the robustness of multi-WLD against different image formats, we also performed experiments with CASIA v2.0, which is larger database and involves images of different formats. Table 11 shows the results with multi-WLD based forgery detection method without and with feature selection. The dimension of the feature vector is 960 with Cb and Cr components and 1920 for FLF case before selection. After feature selection, the dimension is reduced to 379, 185, 359 for the cases of Cb, Cr and FLF, respectively. Figure 13 shows ROC curve of the forgery detection method for CASIA v2.0 using FLF system. The results show that, as in the case of CASIA v1.0, both Cr and FLF yield good results, and FLF results in slightly better detection performance. These results have been obtained using the optimal parameter values that we found using CASIA v1.0. The results also indicate that the forgery detection method is robust against different image formats and the overall detection performance is better than that in case

of CASIA v1.0, this is probably due to the reason that the classifier has more patterns to learn well the structure of tampered and authentic images.

Table 11. Performance of the multi-WLD based forgery detection method on CASIA v2.0.

Selection Information	Component	ACC(%)±Std	AUC± Std	# Features
Without Selection	Cr	96.38 ± 0.36	0.966 ± 0.005	960
	Cb	96.61 ± 0.49	0.969 ± 0.004	960
	FLF	96.28 ± 0.675	0.960 ± 0.008	1920
With Selection	Cr	95.70 ± 0.745	0.958 ± 0.008	185
	Cb	96.29 ± 0.77	0.960 ± 0.008	379
	FLF	**96.52 ±0.583**	**0.970 ± 0.007**	**359**

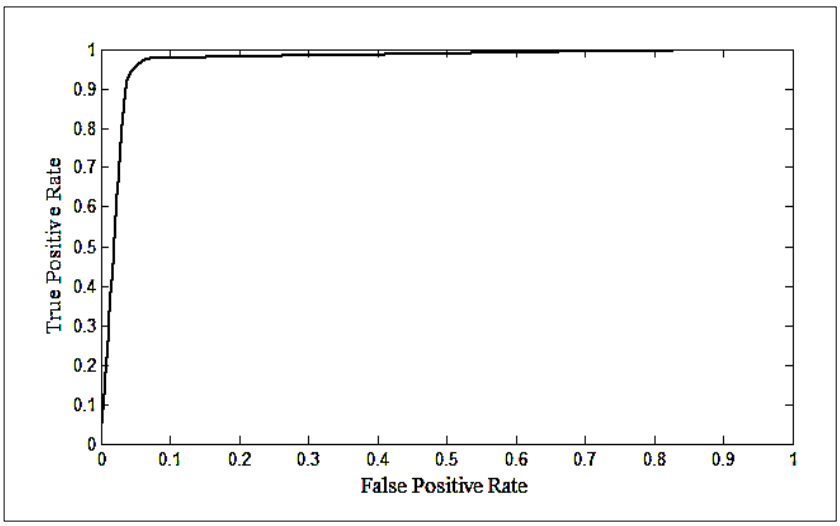

Fig. 13. ROC curve of the multi-WLD based forgery detection method on CASIA v2.0 using FLF case

5.3. *Experiments with Columbia Colour*

To further validate the detection performance of the multi-WLD based forgery detection method, we also performed experiments on Columbia color dataset which is small but contains images of larger size and in TIFF format. Table 12 shows the results for this dataset with feature selection. The multi-WLD based method with FLF achieved 94.17% accuracy, which is better than previously reported best results by the method in [22]. The number of features in FLF after feature selection is 316. These results are comparable with those on CASIA v1.0 and further validate the fact that the method is robust against different image formats.

Table 12. Performance of the multi-WLD based forgery detection method on Columbia dataset

Channel	ACC(%)±Std	AUC± Std	ACC (%) of [22]
Cr	92.50 ± 4.73	0.93 ± 0.05	
Cb	92.78 ± 3.51	0.93 ± 0.05	93.14
FLF	**94.17 ± 3.57**	**0.93 ± 0.05**	

6. Detection Performance with Multi-LBP

In this section, we present the detection results with multi-LBP, which is also a local texture descriptor, for the sake of comparison, for detail see [*]. Different variants of LBP have been considered to show which one performs best for forgery detection. For validation, the experiments were performed on CASIA v1.0.

To see the effect of multi-LBP on forgery detection, we employed SVM with RBF kernel. We examined the effect of different scales (C1-C7) and found that C7 gives better detection performance, so we report only the results with C7. Table 13 presents the results with multi-LBP and chrominance components for forgery detection (i.e. on full dataset) when different LBP variants are used. We notice that the number of features differ due to the type of LBP variant. LBP^{ri} has 4504 features when C7 scale is used without using LLB selection. The number of features decreases with LBP^{u2} to 437 features. LBP^{riu2} has the smallest number of features 42. The best accuracy is obtained with LBP^{u2} and Cr component.

Table 13. Forgery detection results with multi-LBP and chrominance components on full dataset

LBP variants	Feature Selection	Component	Acc(%)±Std	AUC±Std	# Features
LBP^{ri}	Without selection	Cr	85.35 ± 2.77	0.85 ± 0.03	4504
		Cb	84.42 ± 2.87	0.85 ± 0.04	4504
	With selection	Cr	85.41 ± 3.02	0.85 ± 0.03	4495
		Cb	84.30 ± 2.78	0.85 ± 0.04	4414
LBP^{u2}	Without selection	Cr	**86.51 ±3.29**	0.86 ± 0.03	437
		Cb	86.40 ±3.48	0.87 ± 0.03	437
	With selection	Cr	85.93 ±4.95	0.86 ± 0.04	248
		Cb	85.52 ± 2.91	0.86 ± 0.04	274
LBP^{riu2}	Without selection	Cr	80.29 ±3.64	0.80 ± 0.03	42
		Cb	77.56 ± 2.05	0.76 ± 0.03	42
	Without selection	Cr	80.70 ± 3.73	0.81 ± 0.04	38
		Cb	79.48 ±2.26	0.79 ±0.03	34

6.1 Results on Splicing Detection

In this section, we present the results for splicing detection only. Table 14 illustrates the results with different variants of multi-LBP when C7 scale and chrominance components are used. In this case, again LBP^{u2} gives the best result with small number of features 256 features. We notice that small number of features can be used to detect image splicing

due to the nature of forgery. In splicing, there are two different background texture patterns as they come from two different images. Also Cr gives better results than Cb chrominance component on splicing detection. Figure14 demonstrates ROC curves of the detection method based on multi-LBP with different LBP variants and Cr component for spliced images.

Table 14. The results for multi-LBP based splicing detection method

LBP variants	Feature Selection	Component	Acc(%)±Std	AUC±Std	# Features
LBP^{ri}	Without selection	Cr	84.64 ± 4.68	0.84 ± 0.06	4504
		Cb	82.26 ±3.66	0.82 ± 0.05	4504
	With selection	Cr	88.21 ±3.70	0.89 ± 0.05	76
		Cb	86.55 ±3.60	0.86 ± 0.04	117
LBP^{u2}	Without selection	Cr	89.17 ± 3.05	0.89 ± 0.04	437
		Cb	86.07 ±2.69	0.85 ± 0.03	437
	With selection	Cr	**90.36 ±2.94**	**0.90 ± 0.04**	**256**
		Cb	86.55 ±2.81	0.86 ± 0.04	115
LBP^{riu2}	Without selection	Cr	90.24 ± 3.76	0.90 ± 0.04	42
		Cb	86.43 ±3.51	0.87 ± 0.04	42
	With selection	Cr	90.48 ±4.20	0.90 ± 0.05	37
		Cb	86.67 ± 3.96	0.88 ± 0.05	39

6.2 Results on Copy-move Detection

This section gives the results for copy-move detection only. The results are shown in Table 15, it indicates that, as usual, Cr component gives better results than Cb for copy-move detection. Also, LBP^{u2} gives better results than other LBP variants for copy-move forgery. Copy-move forgery detection needs more features as a result of forgery nature where the copied and pasted region is from the same image and the hidden noise pattern remains almost same. Figure15 demonstrates ROC curves of multi-LBP based copy-move detection method with different LBP variants and Cr component.

Table 14. The results for multi-LBP based copy-move detection method

LBP variants	Information Selection	Component	Acc(%)±Std	AUC±Std	# Features
LBP^{ri}	Without selection	Cr	82.64 ± 5.75	0.81 ± 0.05	4504
		Cb	83.33 ± 4.94	0.79 ± 0.08	4504
	With selection	Cr	85.56 ± 4.91	0.83 ± 0.06	1203
		Cb	85.83 ± 5.31	0.83 ± 0.08	3842
LBP^{u2}	Without selection	Cr	**86.81 ± 2.10**	**0.84 ± 0.02**	**437**
		Cb	80.56 ± 4.04	0.77 ± 0.09	437
	With selection	Cr	85.28 ± 3.48	0.81 ±0.04	114
		Cb	80.69 ± 3.49	0.78 ± 0.06	147
LBP^{riu2}	Without selection	Cr	78.06 ± 5.55	0.75 ± 0.08	42
		Cb	73.47 ± 4.70	0.67 ± 0.05	42
	With selection	Cr	75.14 ± 4.65	0.71 ± 0.07	33
		Cb	72.64 ± 3.59	0.66 ± 0.05	34

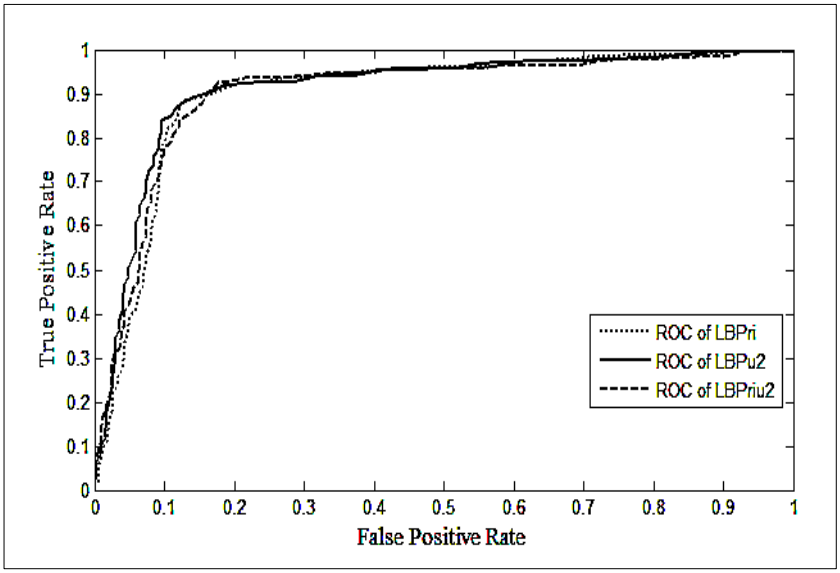

Fig. 14. ROC curves of multi-LBP based splicing detection method with Cr component.

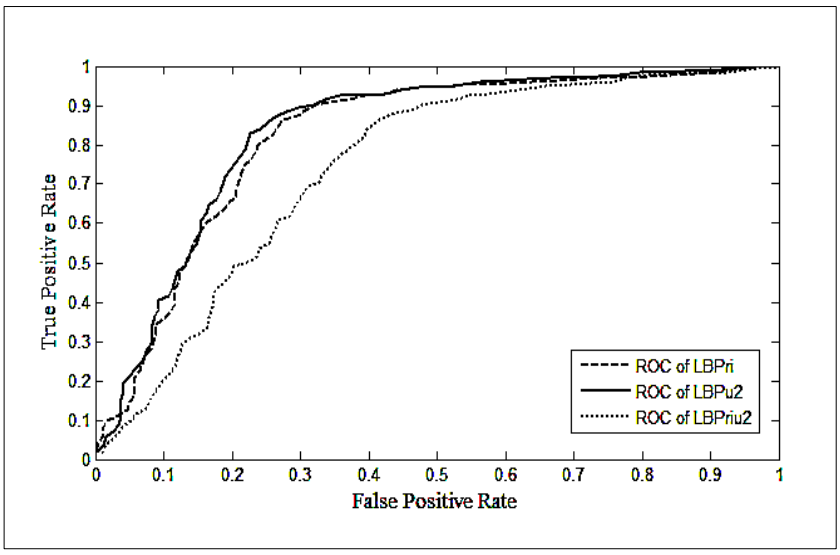

Fig. 15. ROC curves of multi-LBP based copy-move detection method with Cr component.

7 Discussion

Image forgery detection problem has been investigated. Though the tampered image looks natural, the texture micro-patterns go under change, and these tampered traces are

left in the chrominance channels. We investigated the effect of two state-of-the-art local texture descriptors multi-scale WLD and multi-scale LBP for developing a robust system for detecting two types of forgeries (splicing and copy-move forgery). The impact of multi-WLD was investigated thoroughly, and the results presented in previous sections indicate that multi-WLD based method is robust forgery detection method. This method involves different parameters; WLD parameters T = 4, M = 4, S = 20, and scale C7 (which is the concatenation of C1, C2, and C3), and SVM with polynomial kernel give the best results. The experiments were performed on CASIA v1.0 with luminance and chrominance components and their concatenation (FLF), it was found that chrominance component Cr and FLF gave better and almost similar results for splicing detection (i.e. accuracies of 94.29±2.50 and 94.52±1.84, respectively) as well as for copy-move detection (i.e. accuracies of 91.11±3.35 and 90.97±2.72, respectively), but only FLF gave a better result for forgery detection (i.e. accuracy of 94.19±1.60). The detection accuracy for splicing detection is higher than that for copy-move detection, the reason is that in case of copy-move forgery, the copied and pasted regions are from the same image and so the change in texture micro-patterns is less noticeable. Further the experiments were performed to see the robustness of multi-WLD method against transformations (deform, resize, rotate), shapes (arbitrary, circular and rectangular) and sizes (large, medium and small) of copied regions. Also, we performed experiments with CASIA v2.0, which is a larger database and contain images in different formats, the results indicate that multi-WLD method is robust against different image format, and it achieved an accuracy of 96.52±0.58 with FLF. The experiments on Columbia color database gave an accuracy of 94.17±3.57 with FLF.

For the sake of comparison, we also performed experiments with multi-LBP using different LBP variants. The results presented in Section 6 indicate that overall LBP^{u2} gives better results for splicing, copy-move and forgery detection with Cr component and C7 scale, but these results are not better than those with multi-WLD. Figure 16 gives a comparison between multi-WLD, and multi-LBP with different LBP variants for forgery detection. The multi-WLD method is more robust for image forgery detection and gives better accuracy with both Cr and Cb components than multi-LBP on CASIA v1.0. Rotation invariant LBP and uniform LBP give better results than rotation invariant uniform LBP. As the accuracy of multi-WLD with both Cr and Cb is better than that of multi-LBP, so we did not perform experiments with FLF, because there is no chance of improvement.

8 Comparison with other Methods

Multi-WLD based forgery detection method was compared with other recent methods [13, 15, 21]. We implemented the method described in [21] that also uses chrominance components and evaluated it on the full CASIA v1.0 data set using Cr component. The method in [21] obtained 78.53% accuracy, which is much less than 92.62% achieved by the multi-WLD method using Cr component. Table 15 lists the results for splicing, copy-move and forgery (full data set) detection. The method based on multi-WLD outperforms the method [21] and multi-LBP on CASIA v1.0 database. Further it is far superior to other state-of-the-art methods [13, 15] when evaluated on CASIA v2.0.

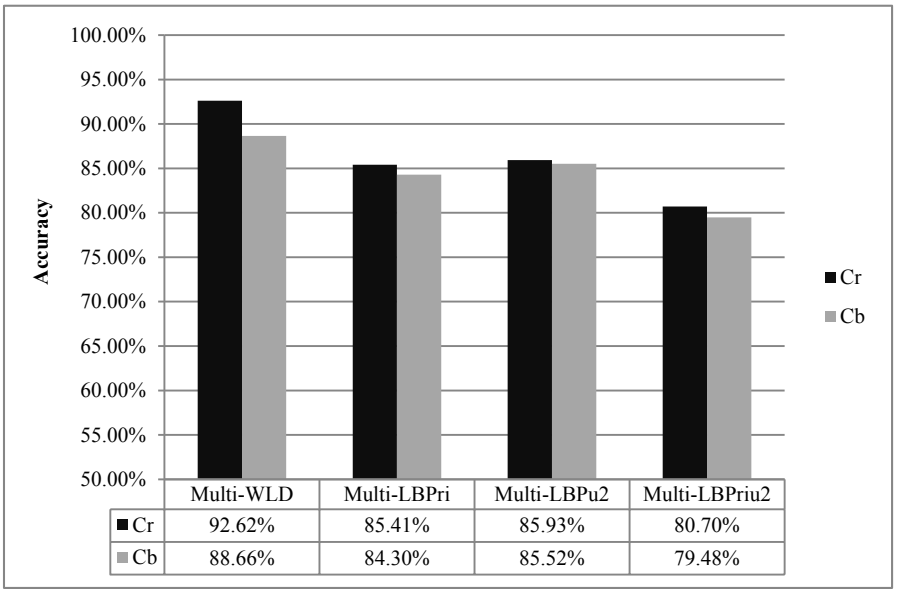

Fig. 16. Comparison between multi-WLD and multi-LBP for forgery detection

Table 15. Performance comparison between different methods

Forgery Type	Dataset Type	Multi-WLD	Multi-LBP	Method [13]	Method [15]	Method [21]
Splicing	CASIA v1.0	**94.29%**	90.48%	-	-	79.90%
Copy-move	CASIA v1.0	**91.25%**	85.56%	-	-	76.30%
Full dataset	CASIA v1.0	**92.62%**	85.93%	-	-	78.53%
Full dataset	CASIA v2.0	**96.52%**	-	84.86%	89.76%	-

9 Conclusion

In an image forgery detection method, the challenging issue is to model the structural changes that take place in an image because of tampering. Assuming that image tampering disturbs the texture micro-patterns in an image and this change can be modeled with texture descriptors, two state-of-the-art local texture descriptors multi-WLD and multi-LBP were employed for image forgery detection. The impact of these descriptors was explored thoroughly and found that multi-WLD outperforms multi-LBP. The features were extracted from the chrominance components of a color image, and SVM was used for classification purpose. The chrominance component Cr performs better than Cb component and SVM with polynomial kernel is better than that with RBF kernel for forgery detection. The best results achieved with multi-WLD based method for forgery detection (i.e. on full dataset) are 94.19% on CASIA v1.0, 96.52% on CASIA v2.0, and 94.17% on Columbia color image databases. These accuracies are better than previously reported results on these datasets. The focus of this work was to identify whether an image is tampered or not, it does not deal with localization problem, i.e. to identify which

region in an image is tampered. A future work is to localize the forgery in a tampered image.

Acknowledgments

This project was supported by NSTIP strategic technologies program number 10-INF1140-02 in the Kingdom of Saudi Arabia. .

References

1. Shivakumar B. and Santhosh Baboo L. D. S. 2010, "Detecting copy-move forgery in digital images: a survey and analysis of current methods," Global Journal of Computer Science and Technology 10.
2. Mahdian B. and Saic S. 2010, "A bibliography on blind methods for identifying image forgery," Signal Processing: Image Communication 25, 389-399.
3. Huang Y., Lu W., Sun W. and Long D. 2011, "Improved DCT-based detection of copy-move forgery in images," Forensic science international 206, 178-184.
4. Cao Y., Gao T., Fan L. and Yang Q. 2012, "A robust detection algorithm for copy-move forgery in digital images," Forensic science international 214, 33-43.
5. Muhammad N., Hussain M., Muhamad G. and Bebis G. 2011, "A non-intrusive method for copy-move forgery detection," in Advances in Visual Computing, ed.^eds. Editior (Springer, pp. Springer.
6. Peng F., Nie Y.-y. and Long M. 2011, "A complete passive blind image copy-move forensics scheme based on compound statistics features," Forensic science international 212, e21-e25.
7. He Z., Sun W., Lu W. and Lu H. 2011, "Digital image splicing detection based on approximate run length," Pattern Recognition Letters 32, 1591-1597.
8. Zhao X., Li J., Li S. and Wang S. 2011, "Detecting digital image splicing in chroma spaces," in Digital Watermarking, ed.^eds. Editior (Springer, pp. Springer.
9. Muhammad G., Hussain M. and Bebis G. 2012, "Passive copy move image forgery detection using undecimated dyadic wavelet transform," Digital Investigation 9, 49-57.
10. Amerini I., Ballan L., Caldelli R., Del Bimbo A. and Serra G. 2011, "A SIFT-based forensic method for copy–move attack detection and transformation recovery," Information Forensics and Security, IEEE Transactions on 6, 1099-1110.
11. Huang H., Guo W. and Zhang Y. 2008, "Detection of copy-move forgery in digital images using SIFT algorithm," in Computational Intelligence and Industrial Application, 2008. PACIIA'08. Pacific-Asia Workshop on, ed.^eds. Editior (IEEE, pp. IEEE.
12. Ling H., Zou F., Yan W.-Q., Ma Q. and Cheng H. 2011, "Efficient image copy detection using multi-scale fingerprints."
13. Shi Y. Q., Chen C. and Chen W. 2007, "A natural image model approach to splicing detection," in Proceedings of the 9th workshop on Multimedia & security, ed.^eds. Editior (ACM, pp. ACM.
14. CASIA image tampering detection evaluation database (CASIA TIDE) v1.0 and v2.0, available at http://forensics.idealtest.org.
15. He Z., Lu W., Sun W. and Huang J. 2012, "Digital image splicing detection based on Markov features in DCT and DWT domain," Pattern Recognition 45, 4292-4299, http://dx.doi.org/10.1016/j.patcog.2012.05.014.
16. Farid H. 2009, "Image forgery detection," Signal Processing Magazine, IEEE 26, 16-25.
17. Chen J., Shan S., He C., Zhao G., Pietikainen M., Chen X. and Gao W. 2010, "WLD: A robust local image descriptor," Pattern Analysis and Machine Intelligence, IEEE Transactions on 32, 1705-1720.

18. Ojala T., Pietikainen M. and Maenpaa T. 2002, "Multiresolution gray-scale and rotation invariant texture classification with local binary patterns," Pattern Analysis and Machine Intelligence, IEEE Transactions on 24, 971-987.
19. Sun Y., Todorovic S. and Goodison S. 2010, "Local-learning-based feature selection for high-dimensional data analysis," Pattern Analysis and Machine Intelligence, IEEE Transactions on 32, 1610-1626.
20. Cristianini N. and Shawe-Taylor J. 2000, An introduction to support vector machines and other kernel-based learning methods. (Cambridge university press).
21. Wang W., Dong J. and Tan T. 2010, "Image tampering detection based on stationary distribution of Markov chain," in Image Processing (ICIP), 2010 17th IEEE International Conference on, ed.^eds. Editior (IEEE, pp. IEEE.
22. Zhao X., Li S., Wang S., Li J. and Yang K. 2012, "Optimal chroma-like channel design for passive color image splicing detection," EURASIP Journal on Advances in Signal Processing 2012, 1-11.
23. Ng T.-T., Chang S.-F. and Sun Q. 2004, "A data set of authentic and spliced image blocks," Columbia University, ADVENT Technical Report, 203-2004, http://www.ee.columbia.edu/ln/dvmm/downloads/.
24. Chang C.-C. and Lin C.-J. 2010, "LIBSVM: a library for support vector machines," http://www.csie.ntu.edu.tw/~cjlin/libsvm.
25. Hussain, M., Muhammad, G., Sahar Q. S., Bebis, G., and Mirza, A. M., "Copy-move Image Forgery Detection using Multi-resolution Weber Descriptors," Proc. SITIS 2012, IEEE Computer Society Press, pp. 395-401, Nov. 25-29, 2012, Naples, Italy.
26. Hussain, M., Muhammad, G., Sahar Q. S, Anwar M. Mirza, Bebis, G.,"Image Forgery Detection Using Multi-Resolution Weber Local Descriptors", Proc. EUROCON 2013, IEEE Computer Society Press, pp. 1570 - 1577, July 1-4, 2013, Zaghreb, Croatia.
27. Sahar Q. S., Hussain, M., Muhammad, G., Bebis, G., "Evaluation of Image Forgery Detection Using Multi-scale Weber Local Descriptors" Lecture Notes in Computer Science, Volume 8034, 2013, pp 416-424, Advances in Visual Computing-Springer, 2014.
28. Hussain, M. Saleh, S.Q., Aboalsamh, H., Muhammad, G., Bebis, G., "Comparison between WLD and LBP descriptors for non-intrusive image forgery detection", Proc. INISTA 2014, IEEE Computer Society Press, pp. 197 – 204, 23-25 June 2014, Alberobello, Italy.